Plasmon-enhanced luminescence in Yb 3 + : Y 2 O 3 thin film and the potential for solar cell photon harvesting

Yalin Lu and Xiaobing Chen

Citation: Applied Physics Letters **94**, 193110 (2009); doi: 10.1063/1.3133340
View online: http://dx.doi.org/10.1063/1.3133340
View Table of Contents: http://scitation.aip.org/content/aip/journal/apl/94/19?ver=pdfcov
Published by the AIP Publishing

Articles you may be interested in

Performance improvement of inverted polymer solar cells by doping Au nanoparticles into TiO2 cathode buffer layer
Appl. Phys. Lett. **103**, 233303 (2013); 10.1063/1.4840319

The effects of energy transfer on the Er3+ 1.54μm luminescence in nanostructured Y2O3 thin films with heterogeneously distributed Yb3+ and Er3+ codopants
J. Appl. Phys. **112**, 063117 (2012); 10.1063/1.4752754

In-situ and ex-situ characterization of TiO2 and Au nanoparticle incorporated TiO2 thin films for optical gas sensing at extreme temperatures
J. Appl. Phys. **111**, 064320 (2012); 10.1063/1.3695380

Near-infrared luminescent and antireflective in SiO2/YVO4:Yb3+ bilayer films for c-Si solar cells
Appl. Phys. Lett. **99**, 121110 (2011); 10.1063/1.3630003

Enhancement of light absorption using high-k dielectric in localized surface plasmon resonance for silicon-based thin film solar cells
J. Appl. Phys. **109**, 093516 (2011); 10.1063/1.3587165

This article is copyrighted as indicated in the article. Reuse of AIP content is subject to the terms at: http://scitation.aip.org/termsconditions. Downloaded to IP: 218.108.88.254 On: Thu, 20 Nov 2014 03:18:04

Plasmon-enhanced luminescence in $Yb^{3+}:Y_2O_3$ thin film and the potential for solar cell photon harvesting

Yalin Lu[1,a] and Xiaobing Chen[2]
[1]*Department of Physics, Laser and Optics Research Center, US Air Force Academy, Colorado 80840, USA*
[2]*College of Physics Science and Technology, Yangzhou University, Yangzhou 225002, People's Republic of China*

(Received 27 February 2009; accepted 22 April 2009; published online 14 May 2009)

Photoluminescence in $Yb^{3+}:Y_2O_3$ thin films grown on sapphire substrates are enhanced using arrays of gold nanoparticles having different shape aspect ratios. The enhanced photoluminescence is attributed to the resonance of localized surface plasmon resonance modes of gold nanoparticles with multiple optical transition lines of the doped Yb^{3+} ions. Its potential as an effective means for solar cell photon harvesting through efficient frequency shifting is also discussed, considering the demonstrated benefits of broad spectral response and much relaxed tolerance for nanofabrication. © *2009 American Institute of Physics*. [DOI: 10.1063/1.3133340]

Major energy loss in a solar cell is due to the nature of the photovoltaic effect. Significant optical energy can be lost because infrared photons in the solar spectrum have insufficient energy to excite an electron to the conduction band (sub-bandgap loss) and because high energy (blue and ultraviolet) photons can raise only one electron to the conduction band, wasting their excess energy through heating the solar cell (thermalization loss). Frequency shifting via downconversion[1] and upconversion using luminescent materials will therefore be useful to "flip" those photons' energies that are either too high or too low back into the suitable energy range of a solar cell. Low frequency conversion efficiency is the main concern due to many reasons including the apparent low intensity from direct solar irradiation.

The signature optical property of a noble metal nanoparticle (NP) is its localized surface plasmon resonance (LSPR), when excited by an electromagnetic (EM) radiation.[2] The peak wavelength of absorption or scattering cross section is highly dependent on size and shape of the NP and its surrounding dielectric properties. The primary consequences of exciting LSPR are selective photon absorption and scattering and local EM field enhancement, which have been investigated for many potential photonic applications on past years.[3] For example, a few orders of magnitude improvement over radiative decay rate is predicted when a metal NP is placed close to a luminescent emitter, permitting an efficient coupling between optical transition dipoles and LSPR modes to occur. In fact, luminescence enhancement was experimentally demonstrated with Er^{3+}-doped materials,[4,5] quantum dots,[6] and dyes.[7]

A Yb^{3+} ion has a relatively simple electronic structure of two energy-level manifolds: a ground $^2F_{7/2}$ state and an excited $^2F_{5/2}$ state, which are separated by $\sim 10\,000$ cm^{-1}.[8] Its broad emission from 0.9 to 1.1 μm will be useful for silicon-based solar cells because the emission range is above the bandgap of Si (~ 1.1 μm). When codoped with terbium ions (Tb^{3+}), efficient cooperative energy transfer from Tb^{3+} ($^5D_4$) to Yb^{3+} ($^2F_{5/2}$) may occur, which will result in an absorption of one blue or ultraviolet photon by one Tb^{3+} ion and then an emission at ~ 1 μm by two Yb^{3+} ions ($^2F_{5/2}$-$^2F_{7/2}$).[9] A Tb^{3+}–Yb^{3+} activator couple could be ideal for realizing an efficient frequency downconversion for Si solar cells. Hence, there is a need to experimentally demonstrate the plasmon-enhanced photoluminescence (PL) in 1 μm wavelength range in Yb^{3+} doped materials, in order to reduce the above-discussed concern over low conversion efficiency.

In this letter, experimental demonstration of the coupling between optically active Yb^{3+} ions and gold (Au) NPs is reported. Highly oriented ytterbium-doped yttria ($Yb^{3+}:Y_2O_3$) thin films were grown on sapphire substrates. Arrays of Au NPs with different shape aspect ratios were further fabricated on above $Yb^{3+}:Y_2O_3$ thin films. Intensity-integrated PL from such samples was recorded, when excited by a Nd^{3+}:YAG (YAG denotes yttrium aluminum garnet) laser's green output. The observed dependences of PL on both NP aspect ratio and the incident polarization reveal a clear PL enhancement assisted by the coupling.

Y_2O_3 is a common host for many luminescent materials. It has a *c*-type cubic structure with a lattice parameter of 10.60 Å. Y_2O_3 shows a broad transmittance from 0.28 to over 8.0 μm, a range broad enough to cover the entire solar spectrum of AM 1.5-G. Yb_2O_3, on the other hand, crystallizes in the same structure as Y_2O_3, with a smaller lattice parameter of 10.43 Å. Y^{3+} and Yb^{3+} are close in ionic radii (90 and 87 pm, respectively). Both oxides are expected to readily form solid solutions. There is no particular limit for doping Yb_2O_3 into Y_2O_3.[10]

Figure 1 shows a x-ray diffraction (XRD) spectrum from a 200 nm thick Y_2O_3 thin film doped with 12.5 at. % Yb^{3+}, grown on a *c*-cut (0001) sapphire by pulsed laser deposition. The used deposition temperature is ~ 700 °C and the oxygen pressure is ~ 100 mTorr. The deposited thin film was annealed at 700 °C for 2 h. The inset in Fig. 1 is an atomic force microscope (AFM) image over a 1×1 μm^2 surface area showing a surface roughness of ~ 15 nm. The XRD spectrum indicates highly (111)-oriented growth of cubic Y_2O_3. Its major (222) diffraction peak appears at $2\theta \sim 28°$, and (0006) peak from sapphire appears at $2\theta \sim 42°$. The strong (111) orientation is probably from overlapping the cubic Y_2O_3's [111] plane (lattice parameter will be ~ 14.9 Å,

[a]Author to whom correspondence should be addressed. Electronic mail: yalin.lu@usafa.edu.

 © 2009 American Institute of Physics

This article is copyrighted as indicated in the article. Reuse of AIP content is subject to the terms at: http://scitation.aip.org/termsconditions. Downloaded to IP: 218.108.88.254 On: Thu, 20 Nov 2014 03:18:04

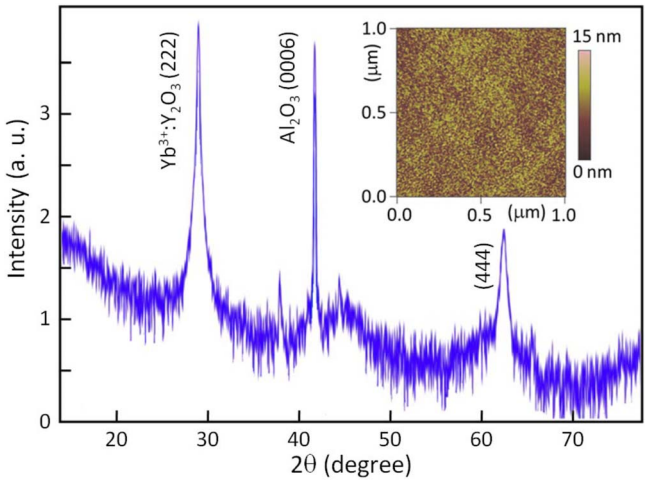

FIG. 1. (Color online) XRD spectrum from a 200 nm thick, 12.5 at. % Yb^{3+} doped Y_2O_3 thin film grown on a *c*-cut sapphire substrate. Inset shows an AFM image of the film over a 1×1 μm^2 surface area.

assuming the cubic lattice parameter is $a=10.60$ Å) with three unit cells along *a*-axis ($a=4.76$ Å) and one unit cell along *c*-axis ($c=12.99$ Å) in sapphire's *c*-plane, with a largest lattice mismatch being ~13.5%.

Room temperature optical absorption and laser-excited emission spectra measured on a ~2 μm thick $Yb^{3+}:Y_2O_3$ film are shown in Fig. 2. This thick film was deposited under conditions similar to those for above thin film. A thick film is required to improve resolution in both absorption and emission measurements. Absorption in the wavelength range from 860 to 1160 nm was measured using a Cary 500 Scan UV-visible-near IR spectrophotometer (SPM). Emission in the range from 915 to 1080 nm was measured by another SPM and using an optical fiber-coupled diode laser (~960 nm) as the excitation source. The absorption spectrum shows three main lines of 977, 960, and 920 nm, and the emission shows four main lines of 1069, 1032, 1020, and 977 nm. Such lines originate from manifolds inside both upper ($^2F_{5/2}$) and ground ($^2F_{7/2}$) levels of the doped Yb^{3+} ions, as the insets show in above Fig. 2.

Gold NPs were fabricated on to the $Yb^{3+}:Y_2O_3$ thin film, following procedures of surface cleaning, spin coating poly(methyl methacrylate) photoresist, electron-beam lithography of the predesigned array patterns, developing the resist, Au evaporation (with a thickness ~40 nm), and finally lift-off. Five arrays were processed, consisting of Au NPs having the same width of ~100 nm, but a varying long axis from 100 to 500 nm at an interval of 100 nm. Inside each array Au NPs were made ~100 nm apart in order to maintain a weak interparticle plasmonic coupling. Scanning electron microscopy (SEM) images from three arrays (with long axes of 100, 200, and 300 nm, respectively) are shown in Fig. 3(a). Figure 3(b) shows the setup used to excite above samples and to record PL spectra. The setup includes a harmonic 532 nm laser beam from a ~1 MHz repetition rate Nd:YAG laser. Laser polarization was selected by a half wave plate to either parallel or perpendicular to the Au NP's long axis. This laser beam was then focused on to the sample by a 60× objective lens. PL spectra was collected from the substrate's bottom side by another 15× objective lens, and recorded by a SPM. A dichroic filter was used in front of the SPM in order to block the green laser light. All recorded PL spectra over the 970–1070 nm wavelength range was integrated and compared to similarly integrated PL from $Yb^{3+}:Y_2O_3$ without Au NPs covering. The use of integration is mainly because of the broadband interest in solar cell applications. The green 532 nm excitation is off from those observed absorption lines of the doped Yb^{3+} ions, therefore a direct excitation of them by the green light will be minimal.

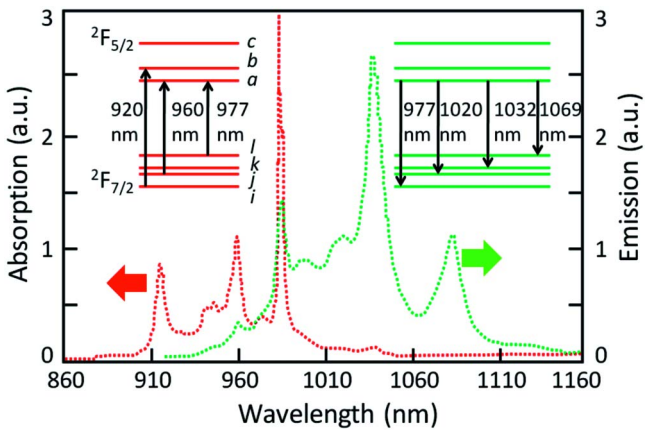

FIG. 2. (Color online) Absorption (red dotted line) and the 960 nm laser excited emission (green dotted line) spectra from a ~2.0 μm thick $Yb^{3+}:Y_2O_3$ film. Insets show major absorption and emission lines originated from transitions among upper and ground manifolds of the doped Yb^{3+} ions.

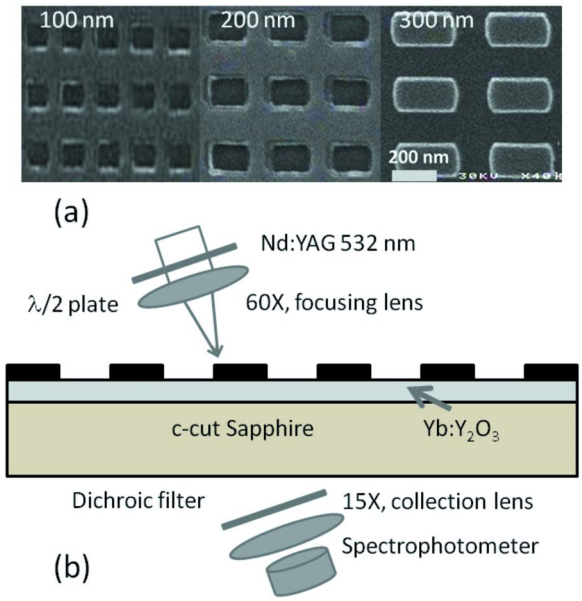

FIG. 3. (Color online) SEM images of Au NPs with long axes of 100, 200, and 300 nm, respectively (a) and schematic of the measurement setup used to record the green 530 nm Nd^{3+}:YAG laser excited luminescence (b).

Dependence of the integrated PL intensity on Au NP's long axis is shown in Fig. 4. Three different laser incidence situations were considered: (1) polarization parallel to the NP's long axis (dotted line connecting red triangles in Fig. 4), (2) polarization perpendicular to the long axis (green circles), and (3) light directly incident on $Yb^{3+}:Y_2O_3$ without NPs (black squares). Using the black squares as reference, a similar trend was found for the case when the incident polarization is perpendicular to the NP's long axis. For the parallel case, a strong luminescence enhancement was observed. Enhancement starts from the NP's long axis at ~150 nm, reaches a maximum somewhere between 200 and

This article is copyrighted as indicated in the article. Reuse of AIP content is subject to the terms at: http://scitation.aip.org/termsconditions. Downloaded to IP: 218.108.88.254 On: Thu, 20 Nov 2014 03:18:04

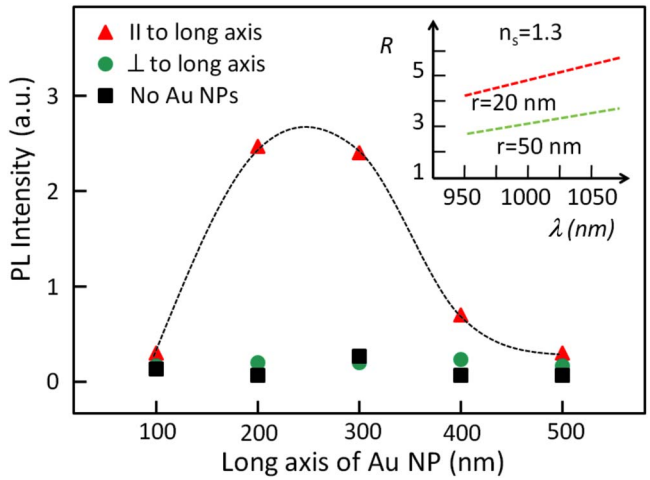

FIG. 4. (Color online) Integrated PL intensity vs the NP long axis. Inset shows the estimated relationship between aspect ratio and the resonance wavelength of LSPR dipoles for two types of nanorods (with $r=20$ and 50 nm) having varying aspect ratios.

300 nm, and then drops back at ~350 nm. This broad size range for Au NPs presenting the luminescence enhancement would be meaningful for solar cell applications, due to the possibility of relaxing tolerance for nanofabrication and reducing overall cost of devices.

The observed PL enhancement can be associated with a coupling of Yb^{3+} $^2F_{5/2}$-$^2F_{7/2}$ transition dipoles with LSPR modes inside Au NPs. It is well known that the LSPR condition will be satisfied when dielectric constants of metal NP and the surrounding medium meet a relationship of $\varepsilon_m(\omega)+Y_i\varepsilon_s(\omega)=0$ (assuming a quasistatic approximation).[11,12] Here Y_i is the depolarization factor, and it relates to the NP shape factor L_1 by $Y_i=(1/L_i)-1$. For Au NP having a prolate spheroidal geometry, Y is >2, increasing as the aspect ratio R (ratio of NP long axis to its short axis) increases. The situation in this research is actually quite complicated. The fabricated Au NPs are rectangular cuboid-like, and they have a similar 40×100 nm^2 side cross section, and a varying aspect ratio of R from 1 to 5. Their dielectric environment is also asymmetric with one side attaching to sapphire, and the remaining sides to air. Therefore, an analytical solution to this geometry will be difficult. To perform a rough analysis, two kinds of nanorods with radius of $r=20$ and 50 nm were considered. A symmetric environment (with an average environment index $n_s\sim1.3$) was also assumed to mimic the actual dielectric asymmetry. Following procedures similar to Ref. 13, relationship between the resonance wavelength of LSPR dipoles and R for both types of nanorods was simulated, and the results are shown as an inset in Fig. 4. Higher order LSPR modes such as quadupoles are neglected. When increasing the wavelength from 950 to 1075 nm, R increases from ~4.2 to ~5.5 for the nanorod having $r=20$ nm, and from ~2.6 to ~3.4 for the $r=50$ nm nanorod. This corresponds to a broad range of nanorod's long axis varying from ~160 to ~340 nm. Apparently, the observed broad NP long axis range presenting a large plasmon-assisted PL enhancement is due to the existence of multiple emission lines from the doped Yb^{3+} ions, which allows a broad-range coupling with many longitudinal LSPR modes that are mainly determined by the NP's long axis.

In conclusion, plasmon-enhanced PL in the wavelength range from 970 to 1070 nm was observed in $Yb^{3+}:Y_2O_3$ thin film through achieving an efficient coupling to the size-varied Au NPs. Existence of multiple transition dipoles of the doped Yb^{3+} ions permits an efficient coupling to multiple longitudinal LSPR modes inside Au NPs, which yields a broad NP size range for strong PL enhancement over a relatively broad spectral range. The results indicate that $Yb^{3+}:Y_2O_3$ is a promising frequency shifting material useful for solar cell photon harvesting.

This research is supported by the U. S. Air Force Office of Scientific Research (AFOSR). Dr. X. B. Chen appreciates the support from the Chinese National Science Foundation (CNSF).

[1]Y. Lu and N. B. Ming, J. Mater. Sci. **30**, 5705 (1995).
[2]S. A. Maier and H. A. Atwater, J. Appl. Phys. **98**, 011101 (2005).
[3]J. Pérez-Juste, I. Pastoriza-Santos, L. M. Liz-Marzán, and P. Mulvaney, Coord. Chem. Rev. **249**, 1870 (2005).
[4]T. Aisaka, M. Fujii, and S. Hayashi, Appl. Phys. Lett. **92**, 132105 (2008).
[5]H. Mertens and A. Polman, Appl. Phys. Lett. **89**, 211107 (2006).
[6]J. B. Khurgin, G. Sun, and R. A. Soref, Appl. Phys. Lett. **93**, 021120 (2008).
[7]J. Gómez Rivas, G. Vecchi, and V. Giannini, New J. Phys. **10**, 105007 (2008).
[8]P. Lacovara, H. K. Choi, C. A. Wang, R. L. Aggarwal, and T. Y. Fan, Opt. Lett. **16**, 1089 (1991).
[9]J. L. Yuan, X. Y. Zeng, J. T. Zhao, Z. J. Zhang, H. H. Chen, and X. X. Yang, J. Phys. D **41**, 105406 (2008).
[10]F. Hanic, M. Hartmanov, G. G. Knab, A. A. Urusovskaya, and K. S. Bagdasarov, Acta Crystallogr., Sect. B: Struct. Sci. **40**, 76 (1984).
[11]A. Oraevsky and A. N. Oraevsky, Quantum Electron. **32**, 79 (2002).
[12]M. M. Miller and A. A. Lazarides, J. Phys. Chem. B **109**, 21556 (2005).
[13]K. S. Lee and M. A. El-Sayed, J. Phys. Chem. B **110**, 19220 (2006).

This article is copyrighted as indicated in the article. Reuse of AIP content is subject to the terms at: http://scitation.aip.org/termsconditions. Downloaded to IP: 218.108.88.254 On: Thu, 20 Nov 2014 03:18:04